Chapter 2. Basic Atomic Physics

Academic and Research Staff

Professor Daniel Kleppner, Professor David E. Pritchard, Professor Wolfgang Ketterle, Dr. Alan L. Lenef, Dr. Fred L. Palmer, Dr. Nicolaas J. van Druten

Visiting Scientists and Research Affiliates

Dr. John R. Brandenberger,[1] Dr. Theodore W. Ducas,[2] Dr. Marek L. Czachor,[3] Dr. Bernd S. Rohwedder,[4] Dr. H. Jörg Schmiedmayer[5]

Graduate Students

Michael R. Andrews, Michael P. Bradley, Michael S. Chapman, Michael W. Courtney, Kendall B. Davis, Joel C. DeVries, Frank DiFilippo, Dallin S. Durfee, Troy D. Hammond, Jeffrey R. Holley, Ljubomir M. Ilic, Hong Jiao, David A. Kokorowski, Dan M. Kurn, Robert I. Lutwak, Marc-O. Mewes, Daniel Ripin, Richard A. Rubenstein, Edward T. Smith, Neal W. Spellmeyer

Undergraduate Students

Ilya Entin, David Garrison, Philip M. Hinz, Everest W. Huang, Amrit R. Pant, Till P. Rosenband, Szymon M. Rusinkiewicz, Charles K. Sestok, Stanley H. Thompson, Peter S. Yesley

Technical and Support Staff

Carol A. Costa

2.1 Studies in Quantum Chaos: Rydberg Atoms in Strong Fields

Sponsors

Joint Services Electronics Program
Grant DAAH04-95-1-0038
National Science Foundation
Grant PHY 92-21489
U.S. Navy - Office of Naval Research
Grant N00014-90-J-1322

Project Staff

Michael W. Courtney, Hong Jiao, Neal W. Spellmeyer, Dr. John R. Brandenberger, Professor Daniel Kleppner

The goal of this research is to understand the structure and dynamics of atomic systems in external fields that are comparable to the interior fields and in which the classical motion may be irregular. Rydberg atoms are central to this research because laboratory fields can be comparable to their atomic fields. In addition, the classical counterparts of these systems often undergo a transition from order to chaos as the field or energy is varied. Consequently, Rydberg atoms in applied fields provide a natural testing ground for studying the (1) connections between quantum mechanics and classical dynamics and (2) quantum behavior of chaotic systems. Our understanding of this system has been advanced by high resolution spectroscopy, development of efficient quantum calculations for atoms in electric and magnetic fields, and theoretical advances in classical dynamics.

Periodic orbit theory provides a unifying principle for relating a quantum spectrum to the periodic orbits of the corresponding classical system in the semiclassical limit. According to periodic orbit theory,

---

1 Professor, Lawrence University, Appleton, Wisconsin.

2 Professor, Physics Department, Wellesley College, Wellesley, Massachusetts.

3 Fulbright fellow, Warsaw, Poland.

4 Universidad Catolica de Chile.

5 Professor, Physics Department, Innsbruck University, Innsbruck, Austria.

each periodic orbit produces a sinusoidal modulation in the density of states. A spherical wave sent out from the origin will recur (overlap with the original outgoing wave) at times corresponding to the periods of the periodic orbits of the classical system. The magnitude of this overlap gives the strength of the spectrum modulation.

In our laboratory, we have recently studied lithium in parallel electric and magnetic fields.[6] In this work, we were concerned with only the low action orbits and ignored differences between hydrogen and lithium caused by the lithium core.[7]

The Hamiltonian of hydrogen in parallel electric and magnetic fields is

$$H = \frac{1}{2}p^2 - \frac{1}{r} + \frac{1}{8}B^2\rho^2 - Fz.$$

This can be rescaled using the substitutions $\tilde{r} = B^{2/3}r$, $\tilde{p} = B^{-1/3}p$, $t = Bt$, and $f = FB^{-4/3}$. The scaled Hamiltonian

$$\tilde{H} = \frac{1}{2}\tilde{p}^2 - \frac{1}{\tilde{r}} + \frac{1}{8}\tilde{\rho}^2 - f\tilde{z}$$

depends only on the scaled energy $\tilde{H} = \varepsilon = EB^{-2/3}$ and scaled field $f = FB^{-4/3}$. Consequently, the classical dynamics also depends only on these two parameters, not on E, F, and B separately. In the limit of large f, this is just the hydrogen Stark system for which the classical motion is regular. As f approaches zero, the system evolves into diamagnetic hydrogen, which is strongly chaotic for $\varepsilon > -0.1$. An examination of the system at intermediate values of f should reveal the system becoming chaotic. We experimentally measured the recurrence spectrum at a scaled energy of $\varepsilon = 0$. At this energy, the system is in the continuum and the motion is unbound.

The scaled action of a particular closed orbit, $\tilde{S}_k = B^{1/3}S_k$, depends only on ε and f. If the spectrum is recorded while the field and the energy are varied simultaneously to keep ε and f constant, the classical dynamics remains the same. This approach has been used previously,[8] but this is its first experimental application to the parallel fields system. An orbit's scaled action and recurrence strength can be obtained directly from the Fourier transform of the spectrum. This Fourier transform is called the recurrence spectrum because *each* peak is located at the scaled action of a periodic orbit, and the height of each peak is proportional to that orbit's recurrence strength.

Our experiment employs a lithium atomic beam that travels along the axis of a split-coil superconducting magnet. A pair of field plates provides an electric field parallel to the atomic beam. Laser beams intersect the atomic beam at a right angle. A 735 nm laser excites the 2S → 3S two-photon transition, and a second laser polarized parallel to the applied fields excites m=0 continuum states that rapidly ionize. The ions are detected by a microchannel plate. To generate a scaled-energy spectrum, the magnetic field is ramped between 0.5 T and 3.0 T while the electric field is varied to maintain f constant. In general, the laser frequency must also be varied to maintain constant ε, but by choosing $\varepsilon = 0$. we could operate at fixed laser frequency. The fractional uncertainty in scaled energy and scaled field are 0.15 percent and 0.2 percent, respectively.

Understanding the experimental spectrum requires a good understanding of the classical dynamics. The traditional tool for studying chaos is the Poincaré surface of section. However, this is not well suited to the continuum where phase space is unbounded and the trajectories rapidly ionize. As an alternative, we have found that the concept of classical ionization time provides a useful signature of the transition from regular to chaotic behavior. Following Main and Wunner,[9] we define the classical ionization time T_{ion} to be the time that an electron excited near the nucleus at an initial angle θ_0 relative to the z axis requires to reach the electric field saddle point. Figure 1 shows how T_{ion} varies with θ_0 for f = 1.0, 0.4, and 0.05.

---

6 H. Jiao, *Experimental and Theoretical Aspects of Quantum Chaos in Rydberg Atoms in Strong Fields,* Ph.D. diss., Dept. of Physics, MIT, 1996.

7 U. Eichmann, K. Richter, D. Wintgen, and W. Sander, *Phys. Rev. Lett.* 61: 2438 (1988); M. Courtney, H. Jiao, N. Spellmeyer, and D. Kleppner, *Phys. Rev. Lett.* 73: 1340 (1994).

8 U. Eichmann, K. Richter, D. Wintgen, and W. Sander, *Phys. Rev. Lett.* 61: 2438 (1988); T. van der Veldt, W. Vassen, and W. Hogervorst, *Europhys. Lett.* 21: 9 (1993); A. Holle, J. Main, G. Wiebusch, H. Rottke, and K.H. Welge, *Phys. Rev. Lett.* 61: 161 (1988).

9 J. Main and G. Wunner, *Phys. Rev. Lett.* 69: 586 (1992).

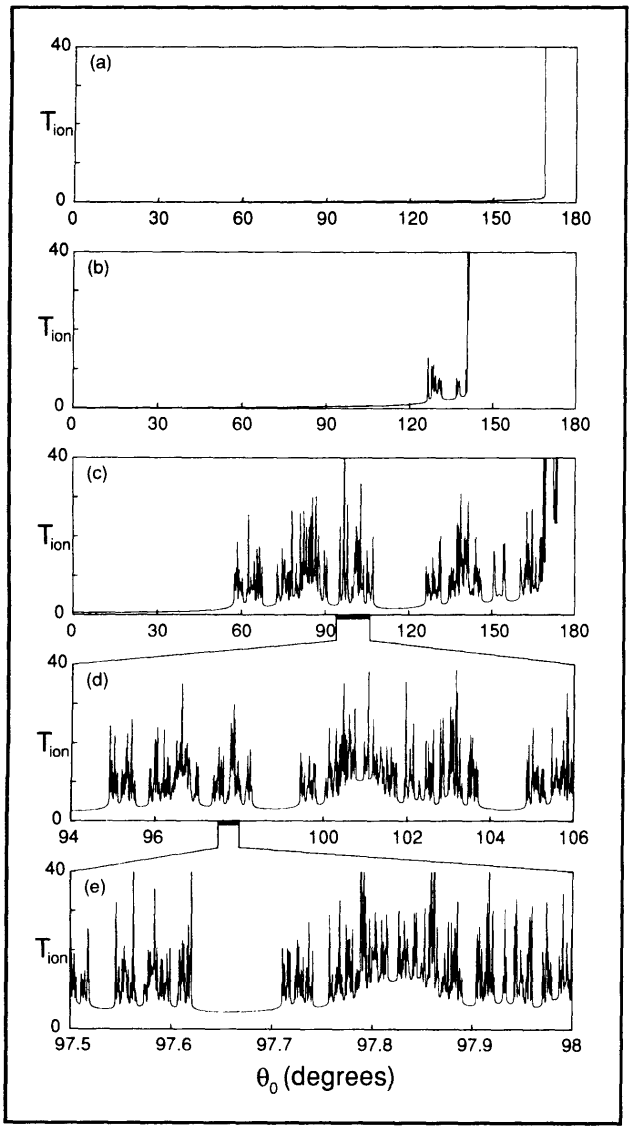

Figure 1. The classical ionization time T_{ion} (in units of scaled time) as a function of the initial angle θ_0 at $\varepsilon = 0$ for various values of f. (a) f = 1.0 , (b) f = 0.4, (c) f = 0.05. (d) and (e) successive blowups of regions indicated.

In the pure Stark problem, the only periodic orbit is the "uphill" orbit, along the axis with θ_0 = 180 degrees. At other angles, the electron leaves essentially immediately. This behavior is seen in figure 1a, except that T_{ion} remains large down to 170 degrees due to the stabilizing effect of the magnetic field. At f = 0.4 (figure 1b), the stable region extends down to about 140 degrees, but below this angle T_{ion} varies erratically for about 15 degrees. At f = 0.05 (figure 1c), the erratic behavior extends to below 60 degrees, with the system displaying wild and random fluctuations. Successive magnifications (figures 1d and 1e) show that the randomly varying pattern extends to ever finer scales: fractal behavior is evident. Similar behavior has been observed in nuclear scattering from model potentials, where the phenomenon has been dubbed chaotic scattering.[10] Following Main and Wunner, we adopt the term *chaotic ionization* to describe the ionization process.

The chaotic ionization process is intimately linked to the existence of closed orbits in the system. Figure 2 shows the locations of closed orbits with scaled action up to $\tilde{S}$ = 10, and T_{ion} as functions of θ_0. The fractal structures appear to be localized near the closed orbits. The closed orbits seem to exert a trapping effect on nearby trajectories: the sensitivity of these trajectories to θ_0 is the source of the fractal behavior in T_{ion}.[11] Because chaotic ionization develops as f approaches zero, we expect to see the development of new closed orbits in the recurrence spectrum of the system. This is what we observe experimentally.

[10] B.P. Koch and B. Bruhn, *J. Phys. A* 25: 3945 (1992).

[11] B. Eckhardt and C. Jung, *J. Phys. A* 19: L829 (1986); C. Jung and H.J. Scholz, *J. Phys. A* 20: 3607 (1987).

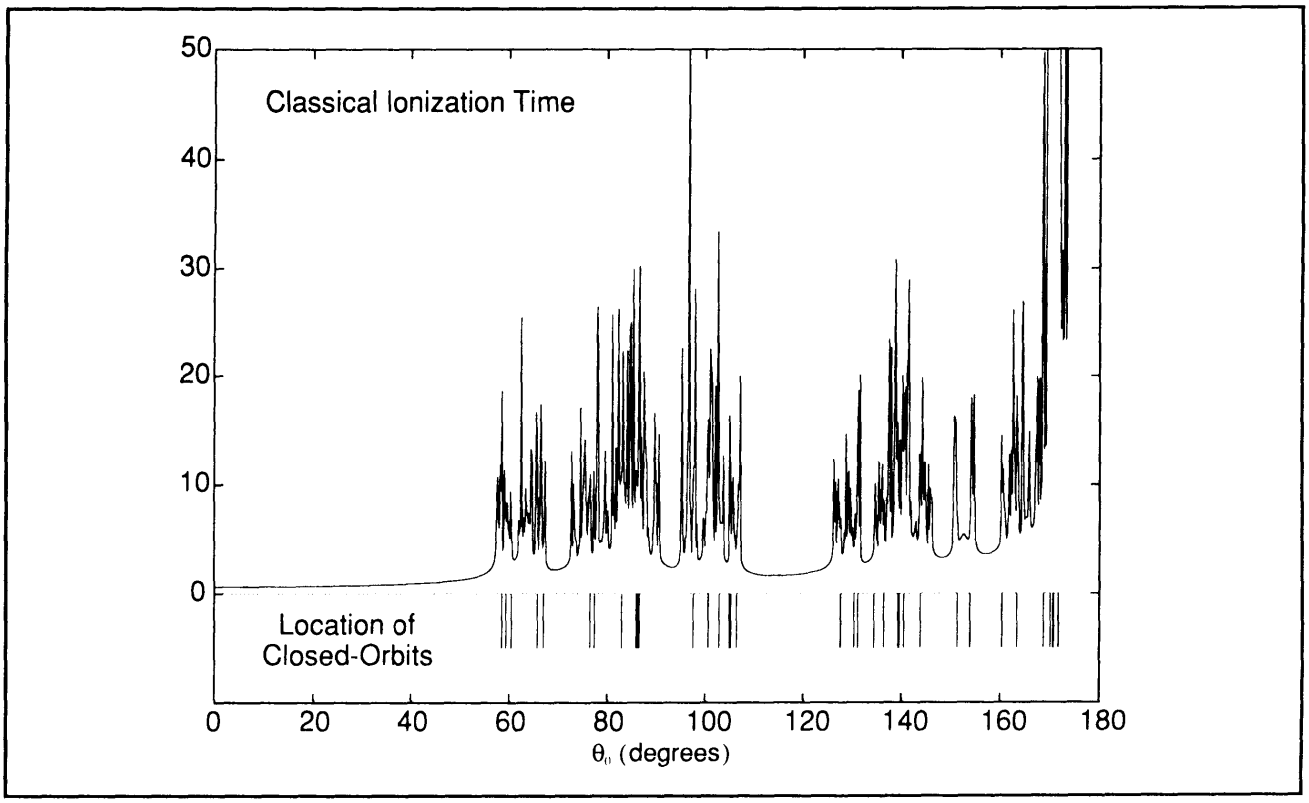

Figure 2. Above: the classical ionization time (in units of scaled time) at $\varepsilon = 0$ and f =0.05. Below: location of closed orbits with $\tilde{S} \leq 10$.

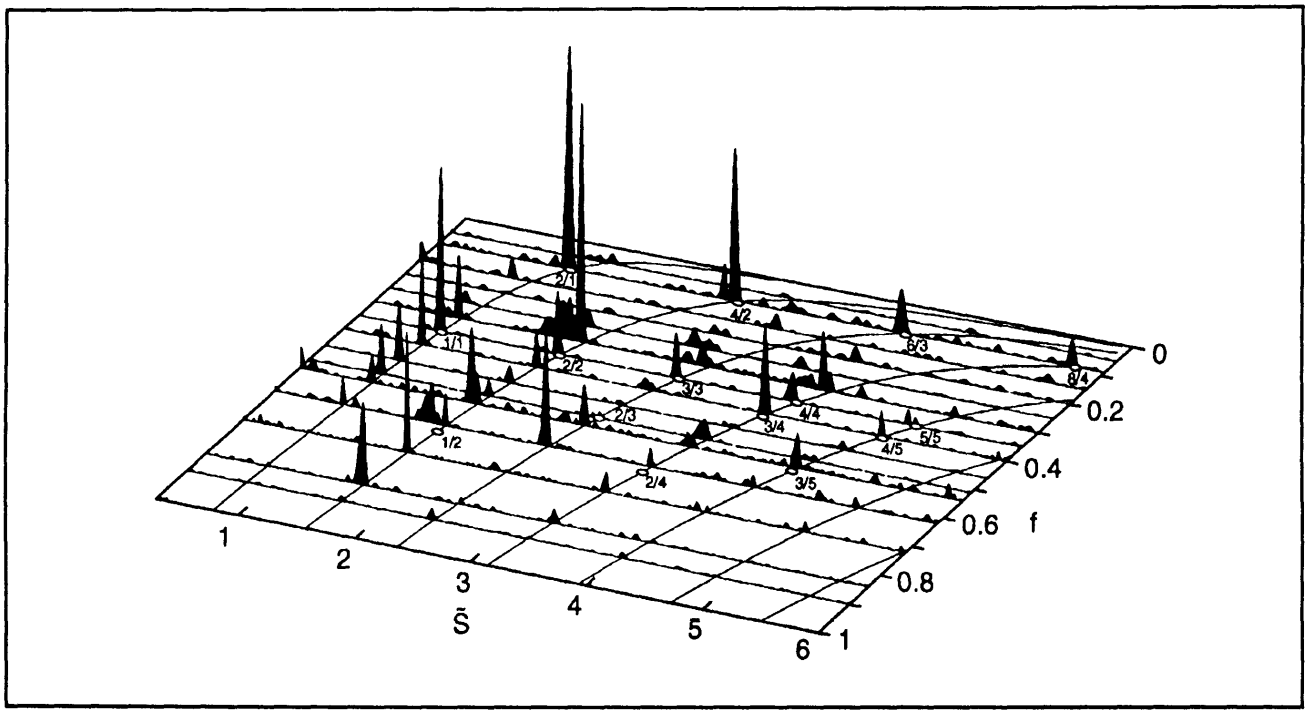

Figure 3. Experimental recurrence spectra at $\varepsilon = 0$ for scaled fields ranging from f = 0.05 to f = 1. The curved lines are the calculated scaled actions of the parallel orbit and its repetitions. Locations of bifurcations are marked with small ovals.

Figure 3 shows experimental recurrence spectra for values of f between 1.0 and 0.05. At large f, the recurrences are those of the parallel "uphill" orbit and its repetitions. As f is reduced, new recurrences become visible. These are created by bifurcations of the parallel orbit and its repetitions. Near the bifurcation points, the orbits often generate large recurrences. This enhancement, caused by the focusing effects of nearby orbits, has been described quantitatively.[12]

In summary, we have shown that one can characterize classical chaos in the continuum through the concept of chaotic ionization, and we have demonstrated that closed-orbit theory provides a natural way to interpret the continuum spectra of a chaotic system. These results help to establish a useful connection between the classical and quantum descriptions of an unbound chaotic system.

In the coming year, we plan to approach this problem in a fundamentally new way: by applying a resonant RF field, we anticipate being able to manipulate individual classical closed orbits in the system. Work is now under way.

2.1.1 Publications

Courtney, M., N. Spellmeyer, H. Jiao, and D. Kleppner. "Classical, Semiclassical, and Quantum Dynamics in the Lithium Stark System." *Phys. Rev. A* 51: 3604 (1995).

Courtney, M., H. Jiao, N. Spellmeyer, D. Kleppner, and J.B. Delos. "Closed Orbit Bifurcations in Continuum Stark Spectra," *Phys. Rev. Lett.* 74: 1538 (1995).

Courtney, M., H. Jiao, N. Spellmeyer, and D. Kleppner. "Long-period Orbits in the Stark Spectrum of Lithium. *Phys. Rev. Lett.* 73: 1340 (1994).

Courtney, M., H. Jiao, N. Spellmeyer, and D. Kleppner. "Quantum Chaos and Rydberg Atoms in Strong Fields." *Proceedings of the Drexel Conference.* Forthcoming.

Shaw, J.A., J.B. Delos, M. Courtney, and D. Kleppner, "Recurrences Associated with Classical Orbits in the Nodes of Quantum Wavefunctions." *Phys. Rev. A* 52: 3695 (1995).

Theses

Courtney, M. *Rydberg Atoms in Strong Fields: A Testing Ground for Quantum Chaos.* Ph.D. diss., Dept. of Physics, MIT, 1995.

Jiao, H. *Experimental and Theoretical Aspects of Quantum Chaos in Rydberg Atoms in Strong Fields.* Ph.D. diss., Dept. of Physics, MIT, 1996.

2.2 Determination of the Rydberg Frequency

Sponsors

Joint Services Electronics Program
Grant DAAH04-95-1-0038
National Science Foundation
Grant PHY 92-21489

Project Staff

Joel C. DeVries, Dr. Theodore W. Ducas, Jeffrey R. Holley, Robert I. Lutwak, Professor Daniel Kleppner

The Rydberg constant, R_∞, relates the wavelengths of the spectrum of atomic hydrogen to practical laboratory units. As such, R_∞ is the natural unit for measurements of atomic energies, and appears as an auxiliary constant in many spectroscopic measurements. Recent advances in optical wavelength metrology have made possible measurements of R_∞ with accuracy approaching 2 parts in 10^{11}.[13] The Rydberg *frequency,* cR_∞, similarly relates the atomic unit of frequency to laboratory units. Although the speed of light c is an exactly defined quantity, the relation between the Rydberg constant and the Rydberg frequency is not merely formal. The precision with which a frequency can be measured is limited in principle to the precision of atomic clocks, which currently exceeds 1 part in 10^{14} and is expected to grow even larger. In contrast, wavelength metrology appears to have reached its limit of precision, somewhat less than 1 part in 10^{11}.

To make full use of the precision of lasers and modern laser spectroscopy and for applications in communications, control, and metrology, we need

---

[12] M. Courtney, H. Jiao, N. Spellmeyer, D. Kleppner, J. Gao, and J.B. Delos, *Phys. Rev. Lett.* 74: 1538 (1995).

[13] T. Andreae et al., "Absolute Frequency Measurement of the Hydrogen 1S-2S Transition and a New Value of the Rydberg Constant," *Phys. Rev. Lett.* 69(13): 1923-1926 (1992); F. Nez et al., "Precise Frequency Measurement of the 2S-8S/8D Transitions in Atomic Hydrogen: New Determination of the Rydberg Constant," *Phys. Rev. Lett.* 69(16): 2326-2329 (1992).

to develop general techniques for measuring the frequency of light. As part of this effort, we propose to help establish an atomic optical frequency scale by measuring the Rydberg frequency directly.

The goals of our experiment are three-fold. First is the re-evaluation of R_∞ itself, providing an independent check, in a different regime and using a totally different technique from previous measurements. Second is the determination of the ground state Lamb shift. Because our method employs high angular momentum states for which the Lamb shift is extremely small and effectively exactly known, our results may be compared with optical measurements of transitions between low-lying states to yield an improved measurement of the Lamb shift. Third is to provide a frequency calibration of the spectrum of hydrogen, enabling the creation of a comprehensive frequency standard extending from the radio frequency regime to the ultraviolet.

Our approach involves measuring the frequency of transitions in atomic hydrogen in a regime where the frequency can be synthesized directly from an atomic clock. The experiment explores transitions between highly excited "Rydberg" states of atomic hydrogen in the neighborhood of n = 29. The transition n=29 → 30 occurs at approximately 256 GHz.

The experiment employs an atomic beam configuration to reduce Doppler and collisional perturbations. Atomic hydrogen is excited to the low angular momentum n=29,m=0 state by a two-step process. The excited atoms are then transferred to the longer lived n=29, m=28 circular state by absorption of circularly polarized radio frequency radiation.[14] The atoms enter a region of uniform electric field in which the frequency of the transition (n=29,m=28)→(n=30,m=29) is measured by the method of separated oscillatory fields. The final state distribution is analyzed by a state-sensitive electric field ionization detector. The resonance signal appears as a transfer of atoms from the n=29 state to the n=30 state as the millimeter-wave frequency is tuned across the transition.

Figure 4 illustrates the main features of the apparatus. Atomic hydrogen or deuterium is dissociated from H_2 or D_2 in a radio frequency discharge. The beam is cooled by collisions with a cryogenic thermalizing channel in order to slow the atoms and thereby increase the interaction time. After the beam is collimated, the atoms pass through two layers of magnetic shielding and an 80 K cryogenic shield before entering the 4 K interaction region. The interaction region is logically divided into three sections: the circular state production region, the separated fields region, and the detection region. These are described briefly below.

In the circular state production region, the hydrogen atoms are excited from the 1s ground state to the $2p_{3/2}$ state, and then to one of the n=29,m=0 states. This takes place in an electric field to provide selective population of one particular n=29, m=0 Stark sub-level. The electric field is then rapidly reduced to an intermediate value as the atoms pass through the center of a circle of four electrodes. These form two pairs of antennas which are fed by a 2 GHz RF source with a 90 degree phase offset. This creates a circularly polarized field that drives the atoms into the n=29, m=28 circular state by the absorption of 28 photons. A pulsed electric field ionization (EFI) detector in the circular state production region monitors the efficiency of the optical excitation and angular momentum transfer processes.

After the atoms are prepared in the n=29 circular state, the beam enters the millimeter-wave separated fields region. Because Rydberg atoms interact strongly with external fields, accurate measurement of the energy level structure requires careful control of the interaction environment. Thermal radiation is reduced by cooling the interaction region to ~ 4 K with a liquid helium flow system. The ambient magnetic field is reduced by the double-wall high-permeability shields. To define the quantization axis, a small electric field is applied with high uniformity by field plates above and below the atomic beam. The millimeter-waves intersect the atomic beam at two locations separated by 50 cm. The millimeter-wave optical system was described in the 1990 *RLE Progress Report.*

The state distribution of the atoms emerging from the interaction region is analyzed by a state-selective electric field ionization detector. Within the detector, the atoms enter a region of increasing electric field produced by a pair of symmetric ramped plates held at constant potential. Atoms in different states are selectively ionized at different fields and the charged nuclei are detected at different positions. The detection electronics record the state and arrival time of each atom to reach the detector. Because the laser system is pulsed, the time resolution of the ionization signal allows contributions to the resonance pattern from each velocity class to be analyzed individually, providing a valuable check on possible systematic errors.

A preliminary resonance measurement was presented in the 1992 *RLE Progress Report.* The pre-

[14] R. Hulet and D. Kleppner, "Rydberg Atoms in 'Circular' States," Phys. Rev. Lett. 51(16): 1430-1433 (1983).

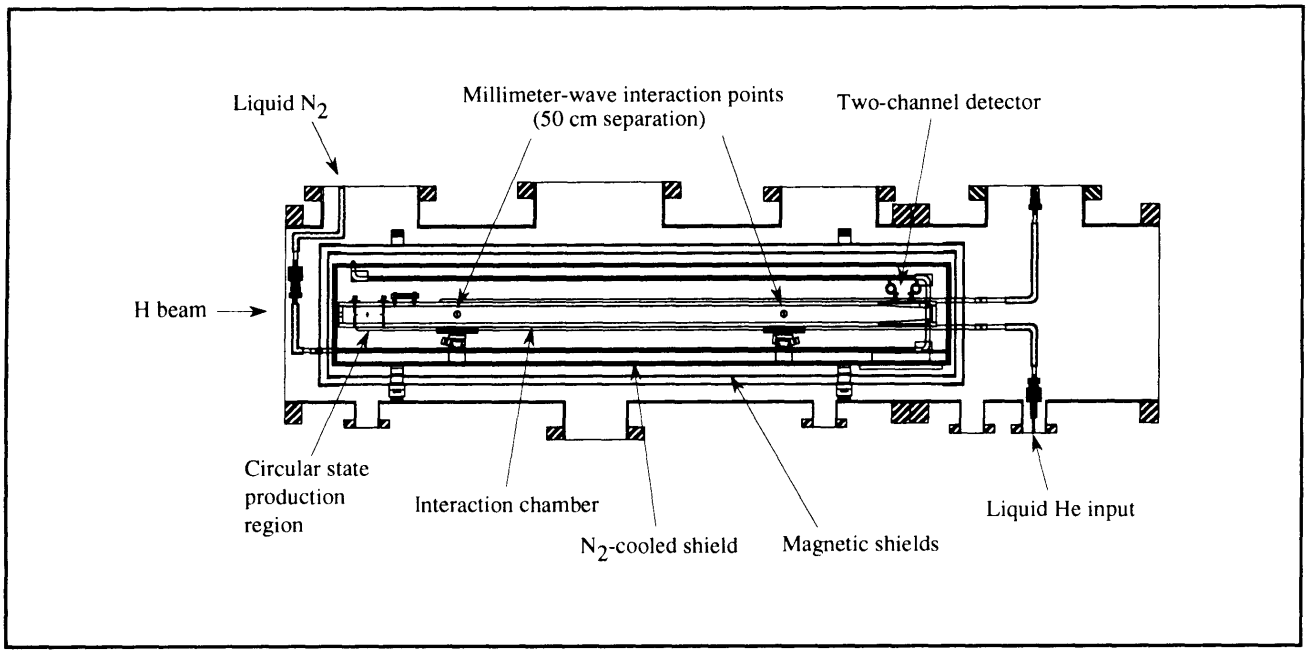

Figure 4. Main chamber of the atomic beam apparatus.

cision of that measurement was limited by low signal levels. Since that time, we have built a second-generation version of the apparatus designed to improve the signal-to-noise ratio by several orders of magnitude. We have completed the new apparatus and have recently begun taking data.

Two accomplishments this year have brought us to the point where we are now beginning to explore the systematics of the new apparatus. The first was the completion and installation of the cryogenically-cooled interaction region. The design of the interaction region was discussed in last year's *RLE Progress Report,* and construction and assembly brought few surprises. The second achievement was the development of the laser system, which is depicted schematically in figure 5.

The laser system consists of two high-power narrow-linewidth dye lasers. The heart of each dye laser is the tunable oscillator, which is shown in figure 6. The gain medium is a quartz cell through which a flourescent dye (DMQ dissolved in P-Dioxane) flows at roughly 3 l/min. The dye is excited by the excimer laser beam which is focused to a line with cylindrical optics. The oscillator cavity is basically of the grazing incidence design,[15] with the addition of an intra-cavity etalon and additional line-narrowing components. The grating-tuning mirror combination acts as a narrow-band mirror, which along with the 60 percent output coupler, defines a plane-parallel Fabry-Perot cavity. The four-prism anamorphic achromatic beam expander provides expansion of 25 times in the horizontal plane which ensures that the 3600 line/mm grating is uniformly illuminated, providing a linewidth of about 0.15 cm^{-1}. The oscillator linewidth is further reduced to about 0.04 cm^{-1} by the intra-cavity etalon. The solid quartz plane-parallel etalon has a free spectral range of 1.3 cm^{-1}. Because the etalon linewidth increases with the divergence of the incident beam, several steps were taken to reduce divergence within the cavity. The prism beam expander reduces the horizontal divergence by a factor of 25 and the pinhole aperture eliminates high order cavity modes. The oscillator frequency is tuned by rotating the grating and the etalon simultaneously along a trajectory which maintains the centering of the etalon mode on the grating line.

[15] M. Littman and H. Metcalf, "Spectrally Narrow Pulsed Dye Laser Without Beam Expander," *Appl. Opt.* 17(14): 2224-2227 (1978).

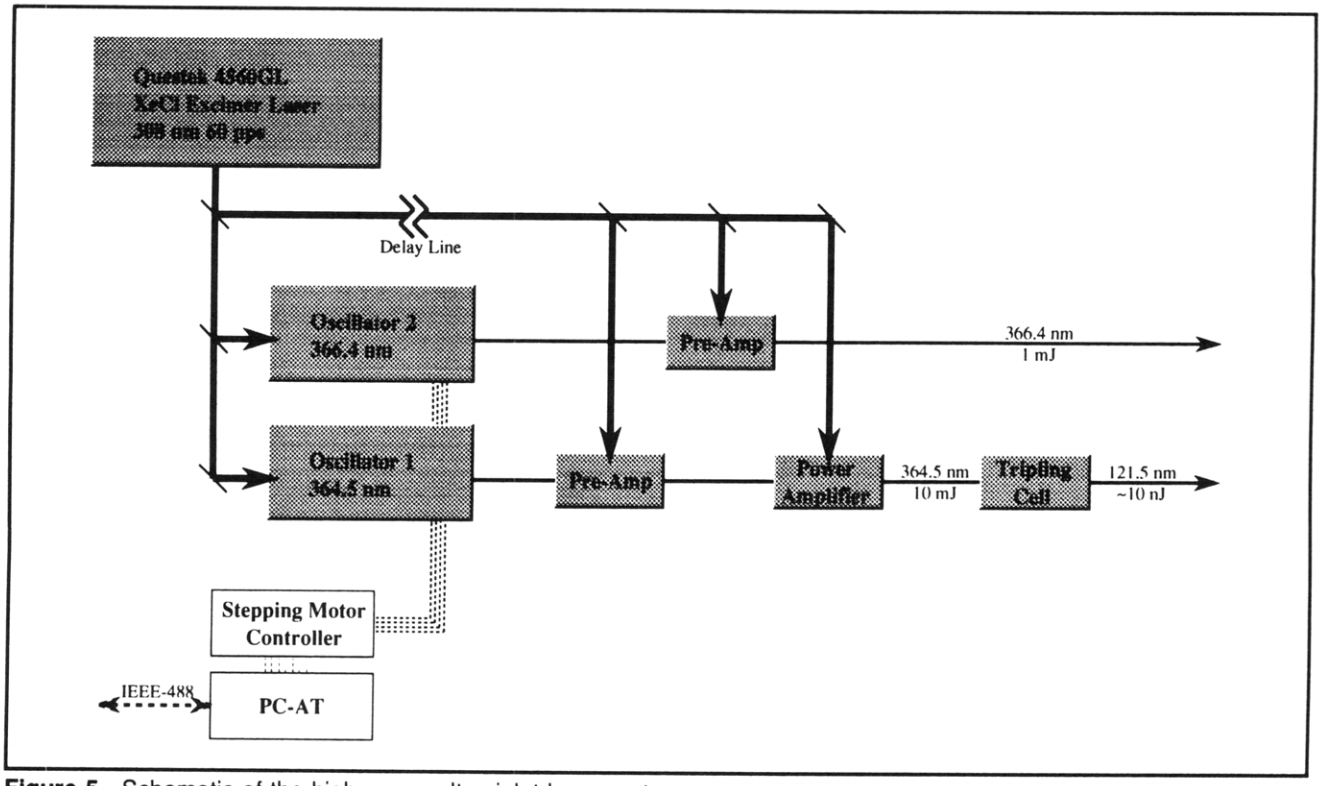

Figure 5. Schematic of the high power ultraviolet laser system.

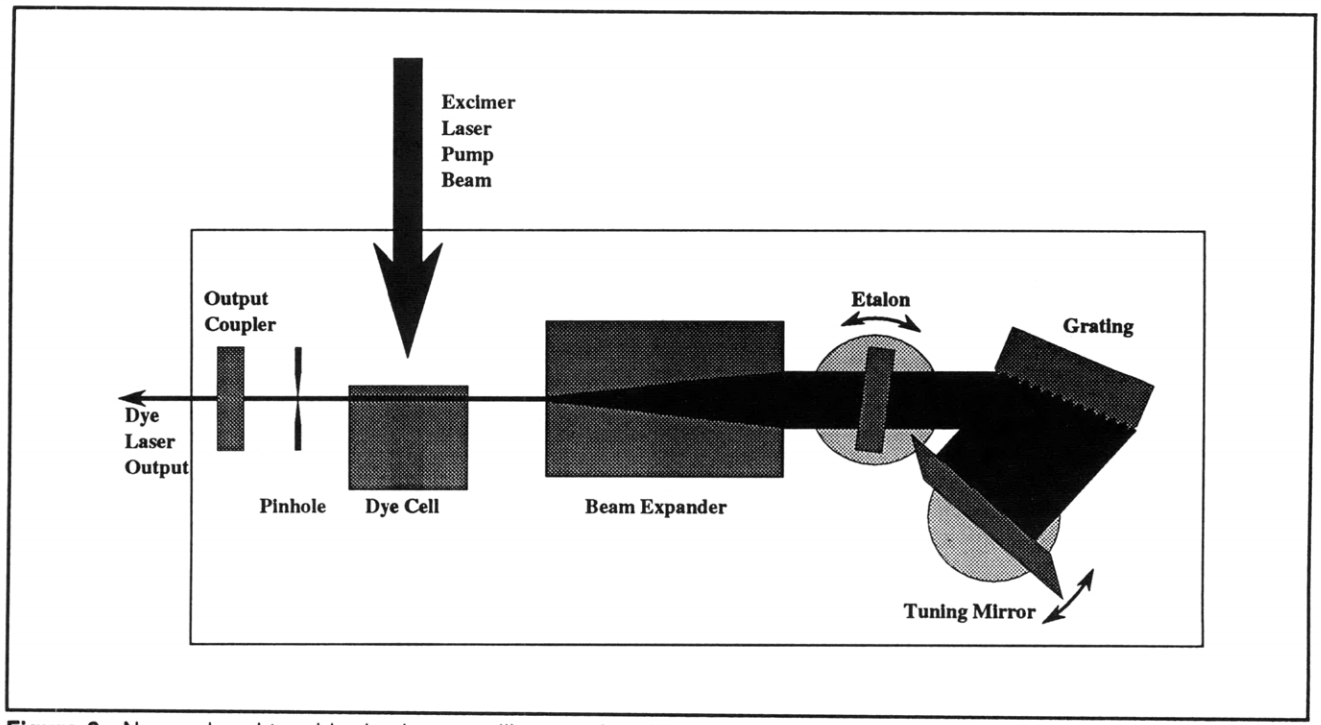

Figure 6. Narrow band tunable dye laser oscillator cavity with intra-cavity etalon.

In order to maintain stability, all fixed oscillator components are rigidly attached to a one-inch thick aluminum base. The tunable components are mounted on double-row high precision industrial bearing sets which are fixed into the base. Because the grating and etalon are quite sensitive to temperature changes, the cavity is enclosed in a plexiglass box and the sensitive components are

actively stabilized to ± 5 mK. The rotating components are driven by 100-pitch lead screws, which push against extended lever arms. An additional 100:1 anti-backlash worm and gear set is incorporated in the grating drive mechanism. The lead screws are turned by stepping motors with 400 steps per revolution, which are driven by the stepping-motor controller. The angular resolution of the drive system is 10 μrad for the etalon and 100 nano-rad for the grating. An AT-compatible personal computer which operates the stepping-motor controller through its parallel printer port maintains the synchronous tuning of the grating and etalon. The controlling software allows for keyboard manipulation of the tuning curves as well as an IEEE-488 interface for remote control of the laser tuning.

The oscillator is pumped by 25 mJ of excimer laser energy and produces roughly 250 μJ of tunable radiation around 364 nm. The tunable radiation is then amplified to 1 mJ in a preamplifier, pumped by an additional 25 mJ of excimer power which is delayed by 5 ns to allow for the oscillator start-up delay. This 1 mJ is sufficient for the $2p \rightarrow n = 29$ laser at 365 nm. The Lyman-α radiation for the $1s \rightarrow 2p$ transition is generated by four-wave mixing of a signal from a laser that is tuned to one-third of the Lyman-α frequency. This signal passes through a second amplifier stage, which is pumped with roughly 150 mJ of excimer power, to produce a 10 mJ pulse at 364.5 nm. The radiation is then focused into a high-purity gas cell containing a phase-matched mixture of krypton and argon gas, where the 364.5 nm radiation is tripled by degenerate four-wave mixing to produce the 121.5 nm Lyman-α radiation.

A typical scan of the Lyman-α laser is presented in figure 7. For this scan the second laser was tuned to the n=70 state of hydrogen. A 10 V/cm electric field was applied to wash out the resonant structure of the upper state. The Lyman-α radiation was then tuned through the $2p_{1/2}$ and $2p_{3/2}$ states while the excited state population was monitored by the pulsed electric field ionization detector located in the circular state production region.

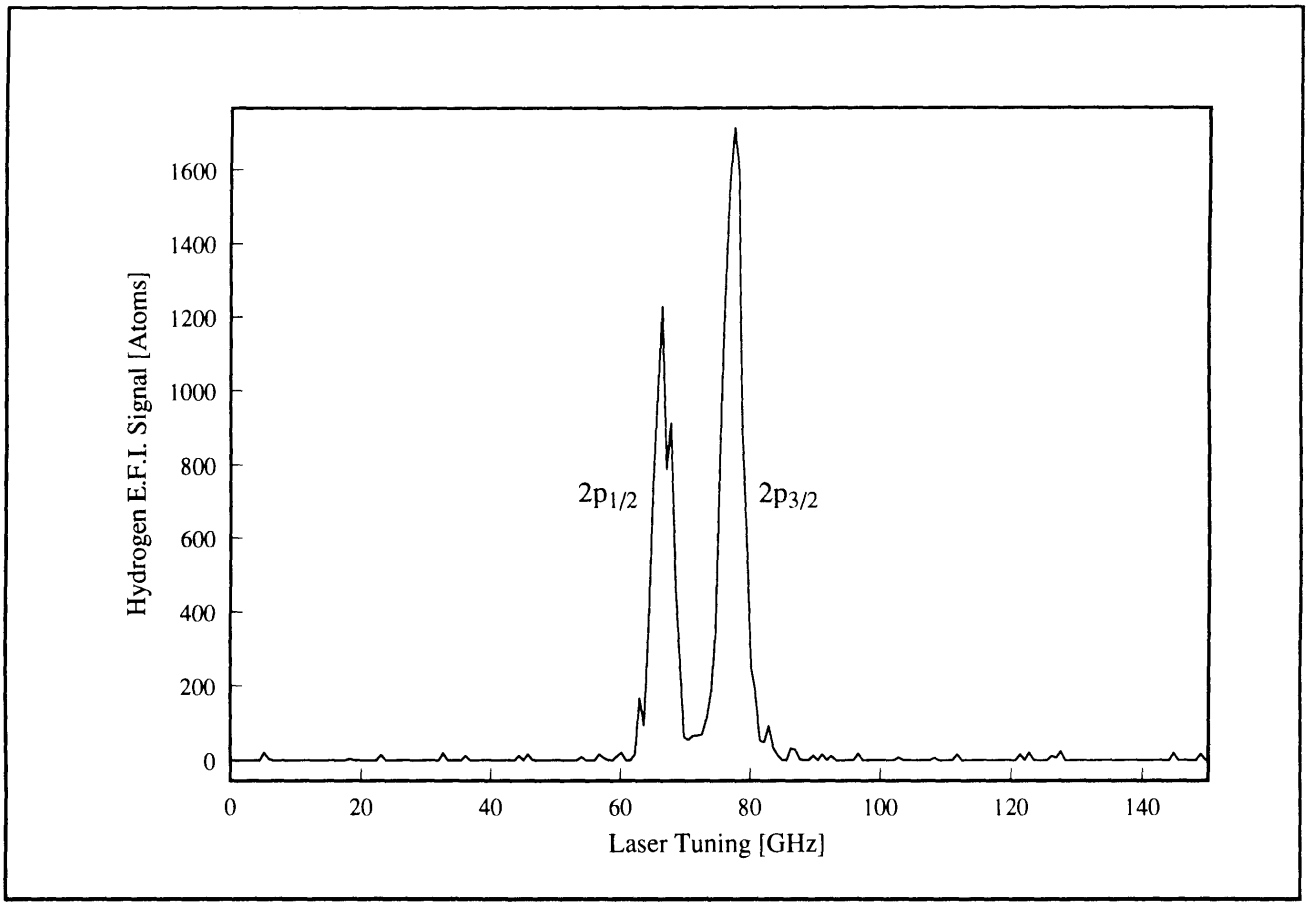

Figure 7. EFI spectrum of the 2p states of atomic hydrogen obtained by two-photon excitation of the n=70 Rydberg state.

Currently, we are fine-tuning the process of transferring the atoms from the n=29, m=0 laser-excited state to the n=29, m=28 circular state. We expect to begin circular-state spectroscopy and to make measurements below the 10^{-10} level this year.

Conference Proceedings

Lutwak, R., J. Holley, J. DeVries, and D. Kleppner, "Millimeter-Wave Measurement of the Rydberg Frequency." *Proceedings of the Symposium on Frequency Standards and Metrology,* Woods Hole, Massachusetts, October 1995.

2.3 Precision Mass Spectrometry of Ions

Sponsors

Joint Services Electronics Program
Grant DAAH04-95-1-0038
National Science Foundation
Grant PHY 92-22768

Project Staff

Michael P. Bradley, David Garrison, Ljubomir M. Ilic, Dr. Fred L. Palmer, Daniel Ripin, Szymon M. Rusinkiewicz, Professor David E. Pritchard

In 1995, we published papers which confirmed that our atomic mass measurements are the most accurate in the world.[16] Our mass table consists of ten atomic masses of particular importance to physics or metrology.[17] The accuracy of these masses, typically 10^{-10}, represents one to three orders of magnitude improvement over previously accepted values. Furthermore, a wide variety of self consistency checks has allowed us to virtually eliminate the possibility of unknown systematic errors. These results contribute to several important experiments in both fundamental and applied physics, including:

- Recalibration of the current x-ray wavelength standard by weighing the energy differences associated with the neutron capture gamma rays of ^{14}N, which are widely used as calibration lines; and
- Determination of the atomic weight of ^{28}Si, part of a program to replace the artifact kilogram mass standard by a crystal of pure silicon, in effect creating an atomic standard of mass.

We have also developed several new techniques that will improve the accuracy and versatility of our apparatus. These include methods for loading a wider variety of ions into the trap, hardware and software for directly controling the amplitude and phase of the the ions' magnetron orbits, the demonstration of a technique for dramatically improving the accuracy of our mass comparisons by comparing two simultaneously trapped ions (to eliminate the problems due to field drift), and the demonstration of a squeezing technique to reduce the influence of thermal noise on the measurements. These advances open the door to another dramatic improvement in mass resolution that would allow:

- Determination of excitation and binding energies of atomic and molecular ions by weighing the associated small decrease in mass, $\Delta m = E_{bind}/c^2$ (we must reach our ultimate goal of a few times 10^{-12} to make this a generally useful technique);
- Determination of the molar Planck constant $N_A\hbar$ by weighing neutron capture γ-rays of silicon or sulphur, whose wavelengths will be measured by a NIST group; this will also provide an independent determination of the fine structure constant;
- Measurement of the $^3H - ^3He$ mass difference, important in ongoing experiments to determine the electron neutrino rest mass;
- Improvement of some traditional applications of mass spectrometry resulting from our orders of magnitude improvement in both accuracy and sensitivity; and
- Determination of the molar Planck constant $N_A\hbar$, by measuring the atomic mass and recoil velocity of an atom that has absorbed photons of known wavelength.

Our experimental approach is to measure ion cyclotron resonance on a single molecular or atomic ion in a Penning trap, a highly uniform magnetic field in which confinement along the magnetic field lines is provided by much weaker electric fields. We monitor the ion's axial oscillation by detecting the currents induced in the trap electrodes using ultrasensitive superconducting electronics

---

[16] F. DiFilippo, V. Natarajan, M. Bradley, F. Palmer, and D.E. Pritchard, *Physica Scripta* T59: 144-54 (1995); F. DiFilippo, V. Natarajan, M. Bradley, F. Palmer, and D.E. Pritchard, in *Atomic Physics 14* (New York: American Institute of Physics, 1995).

[17] F. DiFilippo, V. Natarajan, K. Boyce, and D. E. Pritchard, *Phys. Rev. Lett.* 73: 1481 (1994).

developed for this application.[18] This work in trapping and precision resonance draws on Nobel Prize (1989) winning techniques developed by Dr. Hans Dehmelt at the University of Washington and Dr. Norman Ramsey at Harvard University.

We have developed techniques for driving, cooling, and measuring the frequencies of all three normal modes of ion motion in a Penning trap. Thus we can manipulate the ion position reproducibly to within 30 microns of the center of the trap, correcting for electrostatic shifts in the cyclotron frequency to great accuracy. We use a π-pulse method to coherently swap the phase and action of the cyclotron and axial modes.[19] Therefore, although we detect only the axial motion directly, we can determine cyclotron frequency by measuring the phase accumulated in the cyclotron motion in a known time interval. We can measure the phase of the cyclotron motion to within 10 degrees, leading to a precision of 10^{-10} for a one minute measurement. Our entire ion-making process is fully automated, and the computer can cycle from an empty trap to having a cooled single ion in about three minutes under optimal conditions.

Careful shimming of the electric and magnetic fields allows us to keep our systematic errors well below 5×10^{-11}, but unfortunately, the typical statistical fluctuation in our magnetic field between measurements is 2.4×10^{-10}. Thus even with the ability to achieve ~ 20 alternate loadings of two different ions in one night, our overall accuracy is at best 8×10^{-11} (see figure 8). We have found that the distribution of field variation is not Gaussian, but rather has too many outlying points. This has led us to use a generalization of least squares fitting called robust statistics in which a Hampel estimate is used to deweight outlying points in a manner determined by the observed excess number of outliers. This has eliminated arbitrary decisions about dropping "bad points" from our data sets and has increased the stability of our fits.

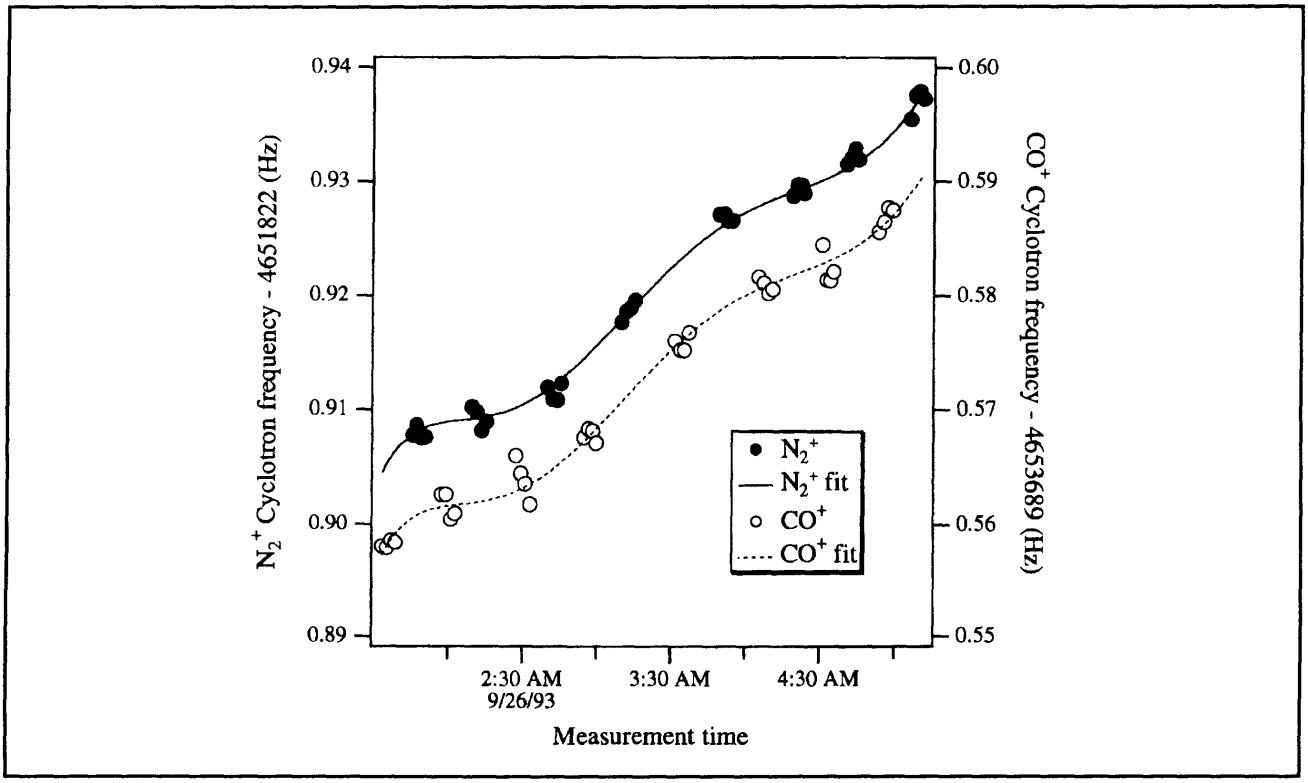

Figure 8. Cyclotron frequency as a function of time for alternate N_2^+ and CO^+ ions in our Penning trap. The frequencies are obtained after a 50s integration of cyclotron phase (see text). The solid line is a polynomial fit to the drift in the field common to both ions.

[18] R. Weisskoff, G. Lafyatis, K. Boyce, E. Cornell, R. Flanagan, Jr., and D.E. Pritchard, *J. Appl. Phys.* 63: 4599 (1988).

[19] E.A. Cornell, R.M. Weisskoff, K. Boyce, and D.E. Pritchard, *Phys. Rev. A* 41: 312 (1992).

We have performed a wide variety of stringent checks for systematic errors. In fact, every mass in the table has been obtained from at least two independent sets of mass ratios. Several of the checks employ our new technique for comparison of non-doublets,[20] pairs of ions whose nominal mass to charge ratios are unequal. This technique represents a significant advance in precision mass spectrometry since it allows us to obtain absolute masses by direct comparison to carbon, which is defined to have an atomic mass of exactly 12. It also provides an absolute check of our accuracy by allowing measurements that should verify known ratios such as N_2^+/N^+ and Ar^+/Ar^{++}. We have compared CD_4^+ and CD_3^+ to C to obtain two independent determinations of the atomic weight of deuterium. The results are consistent with the values for the hydrogen masses we obtained from conventional doublet measurements. An extensive series of checks using only doublet ratios was also performed. These include repeated checks of identical ratios (some interspaced by a significant reduction of our field inhomogeneities), checks of circular ratios (eg., A/B, B/C, and C/A), and checks of related ratios (e.g., CO/N_2 and CO_2/N_2O). The consistency of all these checks practically guarantees that our errors are within the quoted limits.

We have made major advances toward our long term goal of improving our accuracy by more than an order of magnitude, which will be achieved by measuring the cyclotron frequencies of two ions trapped in the same field at the same time to eliminate the problem of field fluctuations, and by using squeezing techniques to reduce thermal noise. We have modified our apparatus to allow excitation and detection of two ions at the same time, and demonstrated the capability of two ion measurements to reduce the effects of field fluctuations (figure 9). We have expanded our previous theoretical understanding[21] of two ion dynamics to include the effects of minute imperfections in the trapping fields, identified particular magnetron orbits where these effects are minimized, and developed hardware and software to place ions in those orbits.

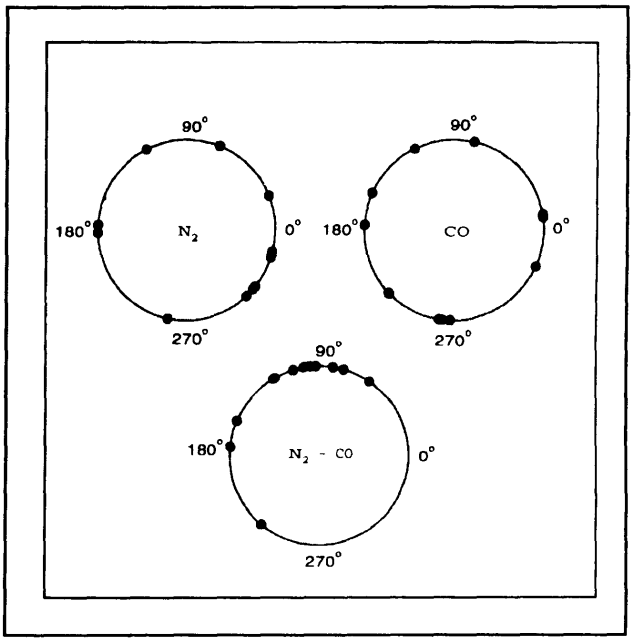

Figure 9. Each dot represents one measured cyclotron phase of simultaneously trapped single N_2^+ and CO^+ ions 16 seconds after excitation. Daytime field fluctuations have virtually randomized the phases of the individual ions but the phase difference between the two remains well defined.

We have also studied the possibility of placing two ions in adjacent traps in case unexpected problems occur when placing them in the same trap. We have evaluated the leading sources of error and designed an arrangement of superconducting coils that will prevent the magnetic fields in the two traps from fluctuating independently.

With either two-ion scheme, the primary source of measurement noise will be the special relativistic mass shift due to thermal fluctuations in cyclotron amplitude. We have proposed several methods of classical squeezing with parametric drives to reduce amplitude fluctuations[22] and demonstrated the simplest of these,[23] reducing thermal noise by about a factor of two.

We have also improved the efficiency and versatility of our basic apparatus. We have built a specialized loader for alkali atoms, as well as an external ion loader with associated ion optics to guide ions into the trap. We have implemented a new signal pro-

---

[20] V. Natarajan, K. Boyce, F. DiFilippo, and D.E. Pritchard, *Phys. Rev. Lett.* 71: 1998 (1993).

[21] E.A. Cornell, K. Boyce, D.L.K. Fygenson, and D.E. Pritchard, *Phys. Rev. A* 45: 3049 (1992).

[22] F. DiFilippo, V. Natarajan, K. Boyce, and D.E. Pritchard, *Phys. Rev. Lett.* 68: 2859 (1992).

[23] V. Natarajan, F. DiFilippo, and D.E. Pritchard, *Phys. Rev. Lett.* 74: 2855 (1995).

cessing algorithm that quickly detects unwanted ions in the trap, and a new data analysis routine that more accurately extracts mass ratios from the data. Finally, we have begun construction of a new detector based on a DC SQUID that will increase our sensitivity by a factor of three or more.

Table 1. Atomic mass table. The center column lists the atomic masses determined from our experiment, and the right column lists the accepted atomic masses from the 1983 evaluation.

Atom	Mass (amu)	Accepted values (amu)
^{1}H	1.007 825 031 6 (5)	1.007 825 035 0 (120)
n	1.008 664 923 5 (23)	1.008 664 919 0 (140)
^{2}H	2.014 101 777 9 (5)	2.014 101 779 0 (240)
^{13}C	13.003 354 838 1 (10)	13.003 354 826 0 (170)
^{14}N	14.003 074 004 0 (12)	14.003 074 002 0 (260)
^{15}N	15.000 108 897 7 (11)	15.000 108 970 0 (400)
^{16}O	15.994 914 619 5 (21)	15.994 914 630 0 (500)
^{20}Ne	19.992 440 175 4 (23)	19.992 435 600 0 (22000)
^{28}Si	27.976 926 532 4 (20)	27.976 927 100 0 (7000)
^{40}Ar	39.962 383 122 0 (33)	39.962 383 700 0 (14000)

2.3.1 Publications

DiFilippo, F., V. Natarajan, M. Bradley, F. Palmer, and D.E. Pritchard. "Accurate Atomic Mass Measurements from Penning Trap Mass Comparisons of Individual Ions." *Physica Scripta* T59: 144-54 (1995).

DiFilippo, F., V. Natarajan, M. Bradley, F. Palmer, and D.E. Pritchard. "Accurate Atomic Mass Measurements from Penning Trap Mass Comparisons of Individual Ions." In *Atomic Physics 14.* New York: American Institute of Physics, 1995.

Natarajan, V., F. DiFilippo, and D.E. Pritchard. "Squeezed States of Classical Motion in a Penning Trap." *Phys. Rev. Lett.* 74: 2855 (1995).

2.4 Atom Interferometry

Sponsors

Charles S. Draper Laboratory
Contract DL-H-4847759
Joint Services Electronics Program
Grant DAAH04-95-1-0038
U.S. Army - Office of Scientific Research
Grant DAAL03-92-G-0229
Grant DAAL01-92-6-0197
U.S. Navy - Office of Naval Research
Grant N00014-89-J-1207

Project Staff

Michael S. Chapman, Troy D. Hammond, Dr. Alan L. Lenef, Edward T. Smith,[24] Richard A. Rubenstein, Dr. H. Jörg Schmiedmayer,[25] David A. Kokorowski, Dr. Marek L. Czachor, Bernd S. Rohwedder, Allen Jordan, Professor David E. Pritchard

[24] Partially supported by a National Science Foundation Fellowship.

[25] Partial support from the University of Innsbruck and an APART Fellowship of the Austrian Academy of Sciences.

Atom interferometers, in which atom or molecular de Broglie waves are coherently split and then recombined to produce interference fringes, have opened up exciting new possibilities for precision and fundamental measurements with complex particles. The ability to accurately measure interactions that displace the de Broglie wave phase has led to qualitatively new measurements in atomic and molecular physics, fundamental tests of quantum mechanics, and new ways to measure acceleration and rotation:

- Atom interferometers permit completely new investigations of ground state properties of atoms and molecules including precision measurements of atomic polarizabilities to test atomic structure models, determination of long range forces important in cold collisions and Bose-Einstein condensation, and measurements of molecular polarizability tensor components.
- Atom interferometers can make fundamental measurements in quantum mechanics. These include measurements of topological and geometric phases, loss of coherence from a reservoir, quantum measurement, and investigations of multiparticle interferometry and entanglement.
- The large mass and low velocities of atoms makes atom interferometers especially useful in inertial sensing applications, both as precision accelerometers and as gyroscopes. They have a potential sensitivity to rotations $\sim 10^{10}$ greater than in optical interferometers of the same area.
- Atom interferometers may have significant applications to condensed matter physics, including measurements of atom-surface interactions and lithography using coherently manipulated fringe patterns that are directly deposited onto substrates.

Our group has pioneered many of these areas, including the first (and only) atom interferometry experiments that employ physically separated paths to make precision measurements. Several major papers have been published this year on a variety of topics underscoring the versatility and usefulness of our interferometer. These topics include quantum coherences,[26] atomic polarizability measurements.[27] index of refraction of matter waves,[28] near field imaging (atomic Talbot effect),[29] molecule optics and interferometry,[30] and a new velocity selection scheme for precision measurements.[31] The investigations have proved to be of widespread general interest to the scientific community and have received many write-ups in the popular scientific press.[32]

During 1995, we made significant improvements to our interferometer's performance, completed experiments in quantum measurement theory, and undertook an experiment demonstrating the high inertial sensitivity of atom interferometers.

---

[26] M.S. Chapman, T.D. Hammond, A. Lenef, J. Schmiedmayer, R.A. Rubenstein, E.T. Smith, and D.E. Pritchard, "Photon Scattering from Atoms in an Atom Interferometer: Coherence Lost and Regained," *Phys. Rev. Lett.* 75: 3783 (1985).

[27] C.R. Ekstrom, J. Schmiedmayer, M.S. Chapman, T.D. Hammond, and D.E. Pritchard, "Measurement of the Electric Polarizability of Sodium with an Atom Interferometer," *Phys. Rev. A* 51: 3883 (1995).

[28] J. Schmiedmayer, M.S. Chapman, C.R. Ekstrom, T.D. Hammond, S. Wehinger, and D.E. Pritchard, "Index of Refraction of Various Gases for Sodium Matter Waves," *Phys. Rev. Lett.* 74: 1043 (1995).

[29] M.S. Chapman, C.R. Ekstrom, T.D. Hammond, J. Schmiedmayer, B.E. Tannian, S. Wehinger. and D.E. Pritchard, "Near Field Imaging of Atom Diffraction Gratings: the Atomic Talbot Effect," *Phys. Rev. A* 51: R14 (1995).

[30] M.S. Chapman, C.R. Ekstrom, T.D. Hammond, R. Rubenstein, J. Schmiedmayer, S. Wehinger, and D.E. Pritchard, "Optics and Interferometry with Molecules," *Phys. Rev. Lett.* 74: 4783 (1996).

[31] T.D. Hammond, D.E. Pritchard, M.S. Chapman, A. Lenef, and J. Schmiedmayer, "Multiplex Velocity Selection for Precision Matter Wave Interferometry," *Appl. Phys. B* 60: 193 (1995).

[32] Articles on recent work performed by our interferometer group have appeared in several journals: J. Maddox, *Nature* February (1995); I. Peterson, *Sci. News,* 147: 116 (1995); P. Yam, *Sci. Am.* 272(4): 30-31 (1995); R. Pool, *Sci.* 268: 1129 May (1995); S. Werner, *Phys. World,* 8(6): 25 (1995); B. Levi, *Phys. Today,* 48(7): 17-18 (1995); P.F. Schewe and B. Stein, *AIP Phys. Bull. on Phys. News,* January 4, 1996; M. Browne, "It's a Molecule. No, It's More Like a Wave," *New York Times* Science Section, August 15, 1995.

2.4.1 Improvements to the Apparatus

This year, we have increased the sensitivity of our apparatus through an improved fabrication process for the 200 nm period de Broglie wave transmission gratings that are its most important component. In collaboration with the Cornell Nanofabrication Facility, where we make our gratings, we have developed a novel registration technique that is capable of producing gratings with phase uniformity over five times the usable area of our old gratings.[33] With the new gratings, we achieve an atom count rate of 200 kcount/sec and a contrast of 17 percent, giving a shot noise limited sensitivity of 5 millirad/$\sqrt{\text{min}}$. We have also fabricated 140 nm and 160 nm period gratings which will further improve sensitivity and allow for separated beam experiments with more massive atoms and molecules. Currently, efforts are underway in the NanoStructures Laboratory here at MIT to develop 100 nm large scale silicon nitride (1 cm^2) gratings with unprecedented phase uniformity using achromatic interferometric (optical) lithography.[34]

2.4.2 Quantum Interference and Coherence

We have investigated the loss of coherence between the two separated de Broglie wave components of our interferometer by scattering resonant photons, λ, in an optically pumped sodium beam. This experiment realized a which-path gedanken experiment contemplated by Feynman[35] and quantifies the transition between coherence and loss of coherence in an interferometer. We measured the fringe contrast due to scattering as a function of separation between the two paths and found that it decreased significantly when the separation exceeded $\lambda/4$, in accordance with the expectations of Bohr's complimentarity principle. Contrast at larger separations, however, exhibited strong revivals (figure 10a), as predicted by our theory. The phase shift of the fringes was also measured and suffered predicted discontinuities (figure 10b).

In an extension of this decoherence experiment, we explicitly showed that scattered photons do not necessarily destroy coherence between the two de Broglie wave components of the interferometer. By using a highly collimated beam and reducing the acceptance angle of our detector, we were able to observe atoms which experienced a photon recoil confined to a small scattering range. For these atoms, we found that the fringe contrast persists over significantly larger path separations than in the previous experiment where all scattering events were detected.

2.4.3 Rotation Sensing

Experiments have been performed to measure both the interferometer's response to rotations as well as its rotational noise, demonstrating the inherent sensitivity of matter-wave interferometers to inertial effects.[36] Small rotations of a few earthrates (earthrate, $\Omega_e = 7.3 \times 10^{-5}$rad/sec) or less were applied to the apparatus, and the resulting interferometer phase measured (figure 11). Since the interferometer has a linear phase response to rotations, a rotation rate was easily inferred and compared to the rotation rate determined from two accelerometers attached to the vacuum housing of our apparatus. A comparison was then made for rotation amplitudes ranging from -4 to $+4$ Ω_e, and plotted in figure 12a.

We have shown the response to have better than 1 percent agreement with theory, and directly observed rotations below 50 $m\Omega_e$ with 20 second integration times. Rotational noise was shot-noise limited for short times (less than two seconds) and was measured to be 13 $m\Omega_e$ in 80 seconds (figure 12b). These results are three orders of magnitude more sensitive than previous measurements of rotation using atom interferometers and demonstrate the promise of using atom interferometers for inertial navigation systems.

---

[33] M.J. Rooks, R.C. Tiberio, M.S. Chapman, T.D. Hammond, E.T. Smith, A. Lenef, R.A. Rubenstein, D.E. Pritchard, and S. Adams, "Coherence of Large Gratings and Electron-beam Fabrication Techniques for Atom-Wave Interferometry," *J. Vac. Sci. Technol. B* 13: 2745 (1995); M.J. Rooks, R.C. Tiberio, M.S. Chapman, T.D. Hammond, E.T. Smith, A. Lenef, R.A. Rubenstein, D.E. Pritchard, and S. Adams, "Coherence and Structural Design of Free-standing Gratings for Atom-Wave Optics," submitted to the *Jap. J. Appl. Phys.*

[34] T.A. Savas, S.N. Shah, M.L. Schattenburg, J.M. Carter, and H.I. Smith, "Achromatic Interferometric Lithography for 100 nm-Period Gratings and Grids," *J. Vac. Sci. Technol. B* 13: 2732 (1995).

[35] R. Feynman, R. Leighton, and M. Sands, "The Feynman Lecture Notes," vol. 3 (Boston: Addison-Wesley, 1966).

[36] A. Lenef, et al, "Rotation Sensing with an Atom Interferometer," to be submitted.

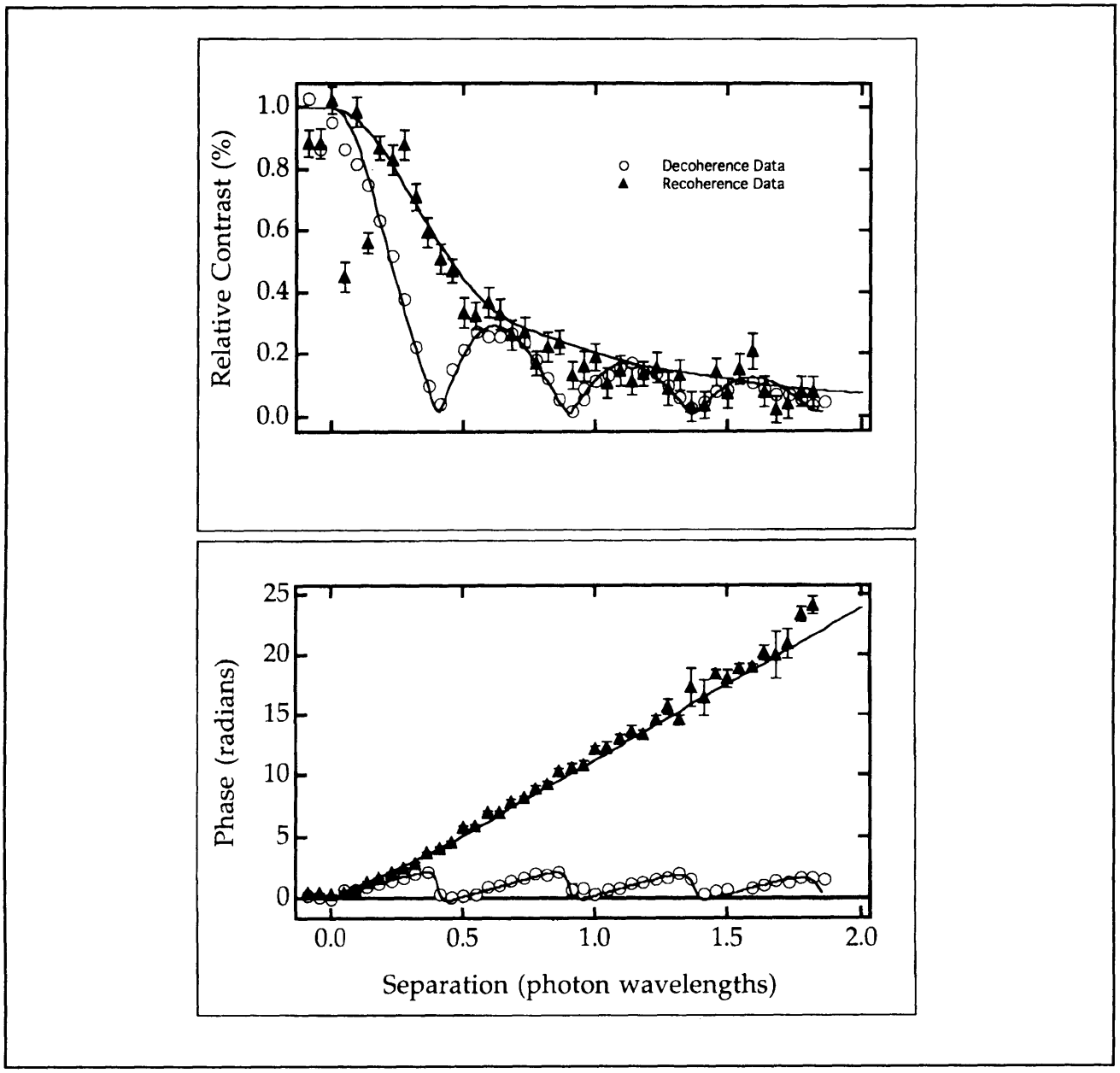

Figure 10. Results of light scattering experiment. (a) Contrast versus separation between de Broglie wave components in units of optical wavelengths. Decoherence data (circles) shows fringe contrast decreasing rapidly, but with revivals. Recoherence data (triangles) show a more gradual decrease in fringe contrast from sub-photon recoil momentum resolved detection of atoms. (b) Phase versus separation between de Broglie wave components in units of optical wavelengths for decoherence data (circles) and recoherence data (triangles).

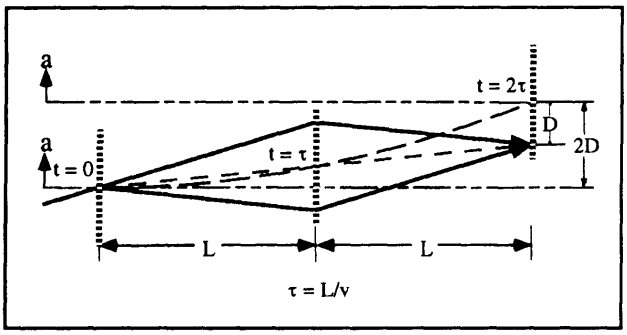

Figure 11. The interferometer in motion under the influence of a transverse acceleration. The atomic beam travels from left to right in the laboratory frame but interacts with the progressively displaced gratings of the moving apparatus. Because a center-line (short dash) between the atom beam paths passes through the middle of the first grating at t = 0, and is offset by a transverse velocity $v_t = 1/2\tau$, it also passes through the middle of the displaced second grating at $t = \tau$. The dashed curve (long dash) represents the displacement of the interferometer due to acceleration. The center-line of the accelerating interferometer is shown (short/long dash) at t = 0, and $t = 2\tau$ where fringes have a relative displacement of -D.

2.4.4 Ongoing Investigations

Longitudinal Momentum Correlations

Recent advances in atom optics and interferometers exploit the transverse coherence of atom sources. Longitudinal coherence is possible, but since atoms with different (but correlated) velocities have different kinetic energies, it is an inherently time dependent phenomenon. Currently, we are pursuing theory with time varying potentials to understand ways to measure, create, and manipulate the longitudinal coherences in our beam.

Understanding and being able to manipulate these coherences will allow us to employ our apparatus to perform studies of a wide range of intriguing time-dependent interactions, including forces which differentially alter the momentum of the atoms in the two legs of the interferometer. One of these, the Anandan force,[37] that arises when a quantum dipole passes through a region of uniform electric and magnetic field, is the subject of considerable theoretical debate.

Velocity Dependent Index of Refraction of a Gas

The refractive index of a gas to passage of a sodium de Broglie wave arises from the collision-induced phase shift between the ground state sodium atoms of the beam and the molecules in the gas cell through which they pass. We plan to extend our recent experiment by varying the incident beam energy, providing a powerful means for further exploration of the intermolecular potentials involved in the collisions.

Dedicated Rotation Sensing Device

The impressive results of our rotation response and noise measurements have motivated the study of a dedicated inertial sensing device based on a high flux atom interferometer with fabricated gratings. Such a device using an effusive Cs beam would produce detected fluxes of about 10^{10} atoms/sec and have a shot noise limited sensitivity of $5 \times 10^{-8}\Omega_e/\sqrt{hr}$.

Velocity Selection through Velocity-multiplexing

The strength of applied potentials in atom interferometry is typically limited because the resulting dispersive phase shifts wash out the interference pattern. In velocity-multiplexing, the velocity distribution of the atomic beam is chopped into a series of narrow peaks such that the velocity dependence of the phase shifts result in rephasing of the interference signal for certain strengths of applied potential. The technique overcomes limitations due to wide and/or poorly known velocity distributions and thus allows a more precise determination of the applied interaction with complete independence from the initial velocity distribution of the beam. We plan to use this scheme to perform experiments requiring precision beyond the 0.1 percent level.

Geometric Phases

Precision measurements of the Aharonov-Casher (AC) phase are planned. This will allow a study of the dependence on the interfering particle's dipole orientation for the first time. Modifications made to our interaction region (a device which allows different potentials to be applied to either arm of the interferometer) to introduce spatially varying magnetic fields will permit investigation of Berry's phase as well.

---

[37] J. Anandan, *Phys. Rev. Lett.* 48: 1660 (1982).

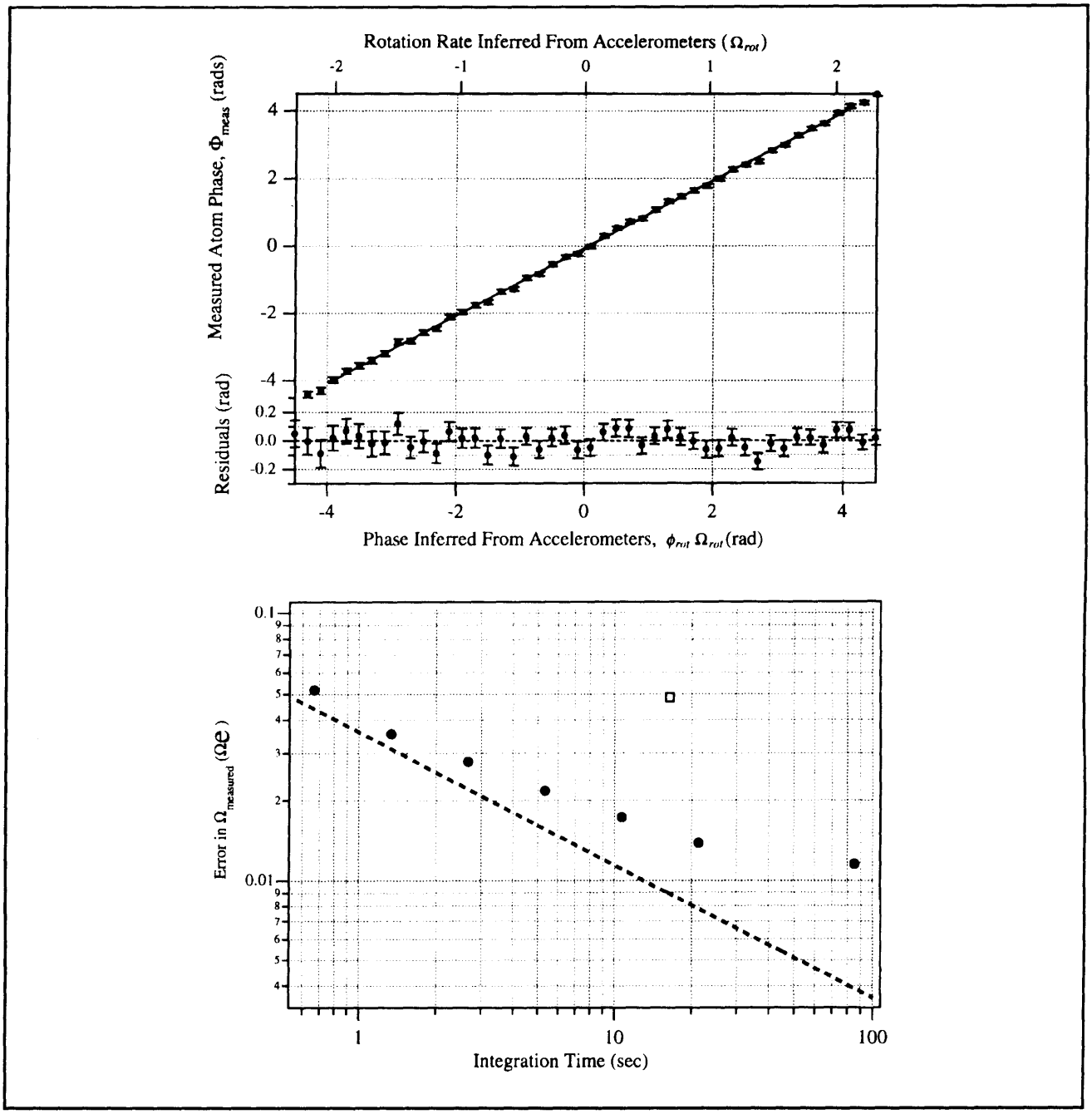

Figure 12. (a) A plot of the measured interferometer phase, ϕ_{meas}, verses the inferred phase from the accelerometer readings, ϕ_{rot}, from a combination of 20 second runs totaling approximately 400 seconds of data (~ 10 sec of data per point). There is a 0.8 percent difference between these measurements with a total error of 1 percent. (b) Reproducibility of the interferometer measurement when driven by a 4.6 Hz sinusoidal motion. The standard deviation of the fluctuations in the measured rotation of the 4.6 Hz spectral peak is plotted verses integration time (circles). This is compared to the shot noise limited error verses integration time (dashed line).

2.4.5 Publications

Chapman, M.S., C.R. Ekstrom, T.D. Hammond, R. Rubenstein, J. Schmiedmayer, S. Wehinger, and D.E. Pritchard. "Optics and Interferometry with Molecules." *Phys. Rev. Lett.* 74: 4783 (1995).

Chapman, M.S., T.D. Hammond, A. Lenef, J. Schmiedmayer, R.A. Rubinstein, E.T. Smith, and D.E. Pritchard. "Photon Scattering from Atoms in an Atom Interferometer: Coherence Lost and Regained." *Phys. Rev. Lett.* 75: 3783 (1995).

Schmiedmayer, J., et al, "Atom and Molecule Interferometry with Separated Beams." In *Atom Interferometry*. Ed. Paul R. Berman, New York: Academic Press. Forthcoming.

Thesis

Chapman, M.S. *Photon Induced Coherence Loss in Atom Interferometry.* Ph.D. diss., Dept. of Physics, MIT, 1995.

2.5 Cooling and Trapping Neutral Atoms

Sponsors

Alfred P. Sloan Foundation
National Science Foundation
Grant PHY 95-01984
U.S. Army Research Office
Contract DAAL01-92-C-0001
U.S. Navy - Office of Naval Research
Grant N00014-90-J-1642
Grant N00014-94-1-0807

Project Staff

Professor Wolfgang Ketterle, Dr. Nicolaas J. van Druten, Michael R. Andrews, Kendall B. Davis, Dallin S. Durfee, Ilya A. Entin, Philip M. Hinz, Everest W. Huang, Dan M. Kurn, Marc O. Mewes, Till P. Rosenband, Charles K. Sestok, Stanley H. Thompson, Peter S. Yesley

2.5.1 Introduction and Summary

Cooling and trapping of neutral atoms offers exciting new possibilities. Many are related to the fact that the deBroglie wavelength increases with decreasing temperature T as $1/\sqrt{T}$. When the deBroglie wavelength is comparable to atomic dimensions (range of the interaction potential), collisions can no longer be treated classically. They are dominated by weak long-range interactions. Dramatic effects happen at even colder temperatures and higher densities, when the deBroglie wavelength becomes comparable to the interatomic spacing. In this case, the atomic waves overlap, and a novel type of highly correlated quantum matter is observed. Fermions would form a correlated Fermi sea where collisions and light scattering are suppressed if most of the final states for these processes are already occupied.

Einstein predicted in 1925 that a gas of bosonic particles will undergo a phase transition into a Bose-Einstein condensate (BEC) if they are cooled to a very low temperature.[38] This new phase is characterized by a macroscopic population of the lowest energy levels. Bose-Einstein condensation is therefore a macroscopic quantum phenomenon like superfluidity and superconductivity. It is distinguished by the coherence of atoms; all atoms in the condensate are indistinguishable and behave identically.

The observation of Bose-Einstein condensation has been one of the major goals in atomic physics in the last few years. This goal has been achieved recently by three groups using different atoms and different techniques.[39] The successful production of Bose condensates is the starting point for a thorough study of this long-sought novel form of matter. The study of Bose-Einstein condensation is important because:

- Bose-Einstein condensation is a paradigm of quantum statistical physics that was predicted more than 70 years ago.[38]
- It becomes possible to perform crucial tests of theories on the weakly interacting Bose condensate. In contrast to other macroscopic quantum phenomena like superconductivity and superfluidity, Bose condensation in atomic gases can be studied at such low densities that

[38] A. Einstein, *Sitzungsber. Preuss. Akad. Wiss.* 18 (1925).

[39] M.H. Anderson, J.R. Ensher, M.R. Matthews, C.E. Wieman, and E.A. Cornell, *Sci.* 269: 198 (1995); C.C. Bradley, C.A. Sackett, J.J. Tollet, and R.G. Hulet, *Phys. Rev. Lett.* 75: 1687 (1995); K.B. Davis, M.-O. Mewes, M.R. Andrews, N.J. van Druten, D.S. Durfee, D.M. Kurn, and W. Ketterle, *Phys. Rev. Lett.* 75: 3969 (1995).

perturbative approaches and mean-field theories are accurate.[40] A detailed theoretical understanding of Bose condensation based on first principles might advance our understanding of more complex systems like liquid helium or high-Tc superconductors.

- A Bose condensate is the ultimate source of ultracold atoms. The kinetic energy of a Bose condensate is on the order of tens of nanokelvin. Such ultracold atoms are ideal for precision experiments (determination of fundamental constants, tests of fundamental symmetries) because the slow motion eliminates most systematic effects. Furthermore, such samples of atoms have potential applications in the field of atom optics, such as the creation of microscopic structures by direct-write lithography or atom microscopy. Structures as small as 65 nm were obtained recently by laser-focused atomic deposition,[41] mainly limited by the transverse collimation and the thermal velocity spread of the atomic beam. Improvements by an order of magnitude should be possible. With ultracold atoms, one could realize the ultimate resolution in focusing atoms. This is analogous to the diffraction limit in optics. A Bose condensate would also find application in metrology, improving frequency standards and atom interferometry. Cesium clocks using microkelvin atoms might improve the accuracy of the current frequency standard by two orders of magnitude.[42] Nanokelvin atoms would offer additional improvements.

- A Bose condensate consists of coherent atoms. Such a state of matter has many analogies with coherent photons or laser light and can be regarded as the first realization of an atom laser. The accumulation of atoms in the Bose condensate can be interpreted as stimulated emission of matter waves. The study of coherent matter waves might become an exciting new subfield of atomic physics.

- A Bose condensate is a novel form of matter with many unknown properties. The ideal (non-interacting) case is well understood, but does not include even the qualitative features of real, weakly interacting systems.[40] In the wake of the progress of the last few years, many theories have been developed on the formation of a condensate, and its collisional and optical properties. Most theories are approximate and have to be tested experimentally. Some theories even lead to contradictory conclusions.

- When a new regime of ultracold temperatures is explored, there is always the hope of finding something completely unexpected!

Despite the rapid progress in laser cooling over the last few years, the closest approach towards BEC was still missing four to five orders of magnitude in phase space density. Laser cooling is limited in the lowest temperature by heating due to spontaneous emission and in density by absorption of scattered light and excited state collisions. Current research activities try to push the limits of laser cooling even further.[43]

Our approach is to use laser cooling as a first step and then continue with evaporative cooling which does not involve light and therefore does not suffer from the above mentioned limitations. The cooling is accomplished by selectively removing atoms with the highest energy from a magnetic trap and then allowing the rest of the sample to rethermalize through elastic collisions. In 1994, we were able to realize for the first time this combination of laser cooling and evaporative cooling.[44] The cooling was limited by trap loss (Majorana flops) in the magnetic trap. In 1995, we could eliminate the trap loss in a novel trap, the optically plugged magnetic quadrupole trap, and cool sodium atoms to Bose-Einstein condensation.

2.5.2 Optically Plugged Magnetic Quadrupole Trap

In 1995, we demonstrated a novel atom trap which consists of a combination of magnetic fields and far-off-resonant light. This trap offers a superior combination of large trapping volume and tight confinement. It allowed us to obtain samples of ultracold atoms at unprecedented densities (10^{14} cm^{-3})

---

[40] K. Huang, *Statistical Mechanics*, 2nd ed. (Wiley, New York, 1987), pp. 286-302.

[41] J.J. McClelland, R.E. Scholten, E.C. Palm, and R.C. Celotta, *Sci.* 262: 877 (1993).

[42] K. Gibble and S. Chu, *Metrologia* 29: 201 (1992).

[43] J. Lawall, S. Kulin, B. Saubamea, N. Bigelow, M. Leduc, and C. Cohen-Tannoudji, *Phys. Rev. Lett.* (1995), forthcoming.

[44] K.B. Davis, M.-O. Mewes, M.A. Joffe, M.R. Andrews, and W. Ketterle, *Phys. Rev. Lett.* 74: 5202 (1995).

and to evaporatively cool atoms to Bose-Einstein condensation.[45]

Evaporative cooling requires an atom trap which is tightly confining and stable. So far, magnetic and optical dipole traps have been used. Optical dipole traps provide tight confinement, but have only a very small trapping volume (10^{-8} cm^3). The tightest confinement in a magnetic trap is achieved with a spherical quadrupole potential (linear confinement); however, atoms are lost from this trap due to non-adiabatic spinflips as the atoms pass near the center where the field rapidly changes direction. This region constitutes a hole in the trap of micrometer dimension. The recently demonstrated TOP trap suppresses this trap loss, but at the cost of lower confinement.[46]

We suppressed the trap loss by adding a repulsive potential around the zero of the magnetic field, literally plugging the hole. This was accomplished by tightly focusing an intense blue-detuned laser that generated a repulsive optical dipole force. The optical plug was created by an argon ion laser beam (514 nm) of 3.5 W focused to a diameter of 30 μm. Heating due to photon scattering was suppressed by using far-off-resonant light, and by the fact that the atoms are repelled from the region where the laser intensity is highest.

The total potential experienced by the atoms is a combination of the dipole potential, the quadrupole trapping potential and the rf dressed atom potential. The latter can be understood qualitatively with a simple argument. At the point where atoms are in resonance with the rf, the trapped state undergoes an avoided crossing with the untrapped states, and as a result the trapping potential bends over. The total potential orthogonal to the propagation direction of the blue detuned laser is depicted in figure 13.

At temperatures above 15 μK, the observed trapped clouds were elliptical with an aspect ratio of 2:1 due to the symmetry of the quadrupole field (figure 14). At the position of the optical plug, there was a hole, which was used for fine alignment. A misalignment of the optical plug by $\sim 20\,\mu$m resulted in increased trap loss and prevented us from cooling below 50 μK. This is evidence that the Majorana spin flips are localized in a very small region around the center of the trap. At temperatures below 15 μK, the cloud separated into two

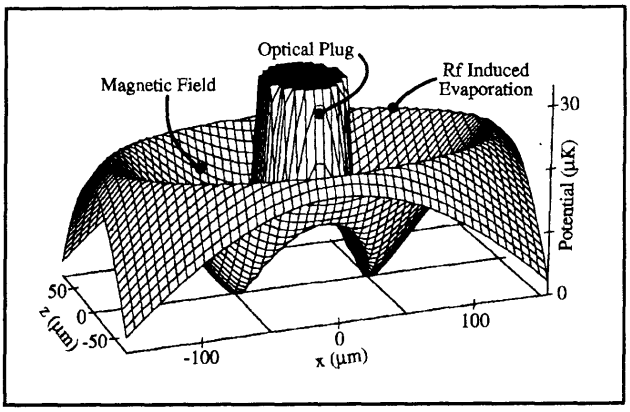

Figure 13. Adiabatic potential due to the magnetic quadrupole field, the optical plug, and the rf. This cut of the three-dimensional potential is orthogonal to the propagation direction (y) of the blue detuned laser. The symmetry axis of the quadrupole field is the z-axis.

pockets (see figure 14b) at the two minima in the potential of figure 13.

2.5.3 Bose-Einstein Condensation of Sodium Atoms

We have recently observed Bose-Einstein condensation in a dilute gas of sodium atoms.[45] The atoms were trapped in the optically plugged magnetic quadrupole trap and cooled by evaporation. The essential condition for evaporative cooling is that the collision rate be sufficiently high for many collisions to occur within the lifetime of the atoms in the trap. Beside high initial density and long trapping times, evaporative cooling requires a method for selectively removing hot atoms from the trap. In rf induced evaporation, atoms are spin-flipped to an untrapped state when they are in resonance with an applied rf field (figure 15). Since this resonance frequency is a function of magnetic field B, atoms are selectively removed at a specific value of B. In the case of transitions between magnetic sublevels m_F, the resonance frequency is $\omega r_f = g\,\mu_B B/\hbar$, where g is the g-factor and μ_B the Bohr magneton. Since the trapping potential is given by $m_F|g|\mu_B B(r)$, only atoms which have a total energy $E > \hbar\omega_{rf}|m_F|$ will evaporate. Evaporative cooling is forced by lowering the rf frequency. Within seven seconds, this reduced the temperature by a factor of 100, and increased the phase space density by six orders of magnitude, leading to Bose-Einstein condensation of the remaining atoms.

---

[45] K.B. Davis, M.-O. Mewes, M.R. Andrews, N.J. van Druten, D.S. Durfee, D.M. Kurn, and W. Ketterle, *Phys. Rev. Lett.* 75: 3969 (1995).

[46] W. Petrich, M.H. Anderson, J.R. Ensher, and E.A. Cornell, *Phys. Rev. Lett.* 74: 3352 (1995).

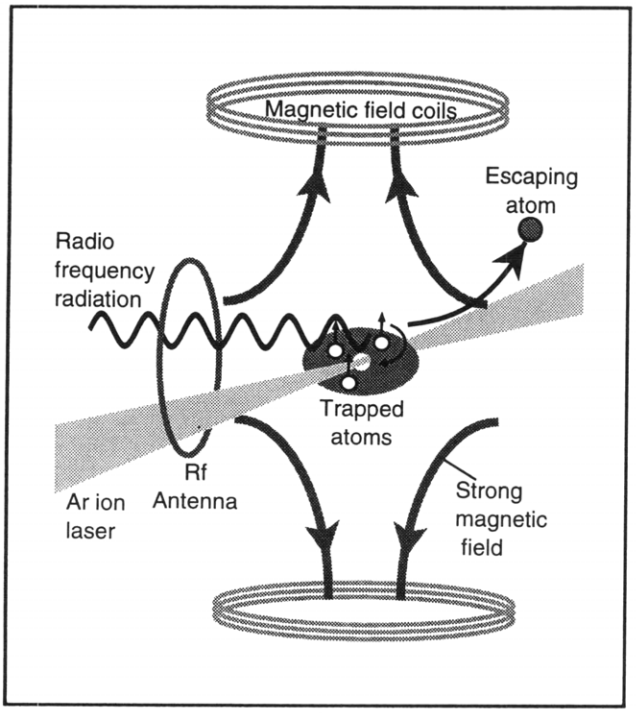

Figure 14. Absorption images of atom clouds trapped in the optically plugged trap. Cloud (a) is already colder than was attainable without the plug (Ar ion laser beam). Cloud (b) shows the break-up of the cloud into two pockets in the two minima of the potential in figure 13. The size of cloud (c) reaches the optical resolution of the imaging system (< 10 mm) still absorbing 90 percent of the probe light. This sets an upper bound on temperature ($< 10\,\mu$K) and a lower bound on density (5×10^{12} cm^{-3}).

Condensates contained up to 5×10^5 atoms at densities exceeding 10^{14} cm^{-3}. The striking signature of Bose condensation was the sudden appearance of a bimodal velocity distribution when the sample was cooled below the critical temperature of $\sim 2\,\mu$K. The distribution consisted of an isotropic thermal distribution and an elliptical core attributed to the expansion of a dense condensate (figure 16).

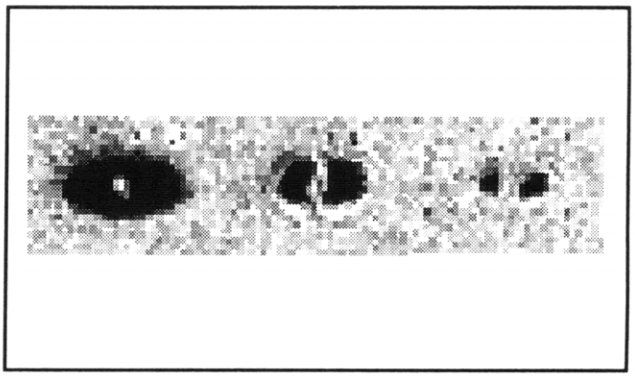

Figure 15. Experimental setup for cooling atoms to Bose-Einstein condensation. Sodium atoms are trapped by a strong magnetic field, generated by two coils. In the center, the magnetic field vanishes, allowing the atoms to spin-flip and escape. Therefore, the atoms are kept away from the center of the trap by a strong (3.5 W) laser beam (optical plug) which exerts a repulsive force on the atoms. Evaporative cooling is controlled by radio-frequency radiation from an antenna. The rf selectively flips the spins of the most energetic atoms. The remaining atoms rethermalize (at a lower temperature) by collisions among themselves. Evaporative cooling is forced by lowering the rf frequency.

This experiment was one of three independent approaches which succeeded in creating BEC in the last few months.[47] Our results on sodium are distinguished by a production rate of Bose condensed atoms which is three orders of magnitude larger than in the two previous experiments. Densities higher than 10^{14} atoms/cm^3 exceed previous results by more than a factor of ten and are promising for the study of collisions and interactions of dense ultracold atoms.

We are currently preparing experiments to study the shape, stability, and optical properties of the condensate. Of special interest are experiments which might reveal the coherent nature of the atoms. Such experiments could be coherent excitations of the condensate by modulating the trapping potential,[48] and interference between two condensates.[49]

---

[47] M.H. Anderson, J.R. Ensher, M.R. Matthews, C.E. Wieman, and E.A. Cornell, *Sci.* 269: 198 (1995); C.C. Bradley, C.A. Sackett, J.J. Tollet, and R.G. Hulet, *Phys. Rev. Lett.* 75: 1687 (1995); K.B. Davis, M.-O. Mewes, M.R. Andrews, N.J. van Druten, D.S. Durfee, D.M. Kurn, and W. Ketterle, *Phys. Rev. Lett.* 75: 3969 (1995).

[48] P.A. Ruprecht, M.J. Holland, K. Burnett, and M. Edwards, *Phys. Rev. A* 51: 4704 (1995).

[49] J. Javanainen and S.M. Yoo, *Phys. Rev. Lett.* 76: 161 (1996).

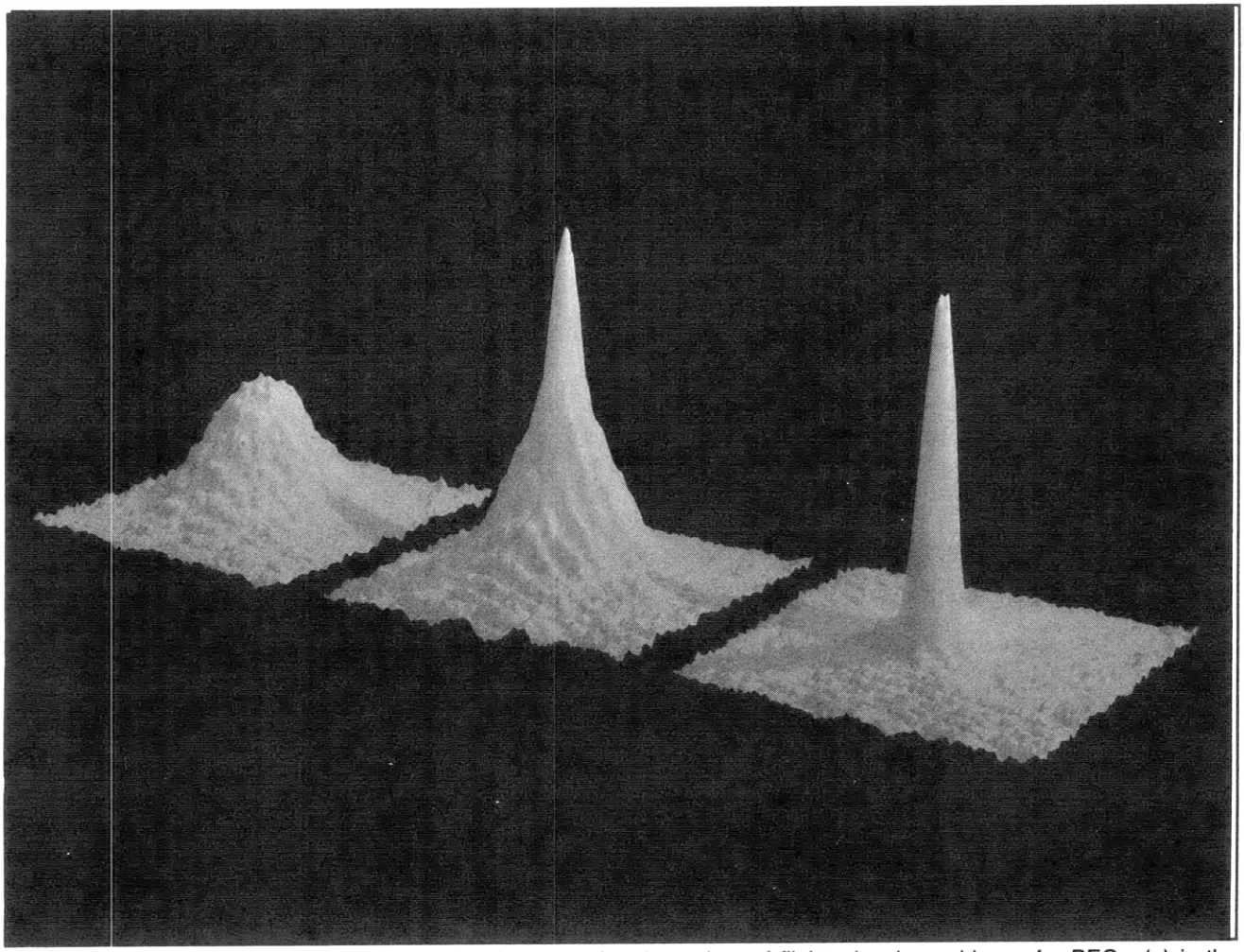

Figure 16. Two-dimensional probe absorption images, after 6 ms time of flight, showing evidence for BEC. (a) is the velocity distribution of a cloud cooled to just above the transition point, (b) just after the condensate appeared, (c) after further evaporative cooling has left an almost pure condensate. The figure shows the difference between the isotropic thermal distribution and an elliptical core attributed to the expansion of a dense condensate. The width of the images is 0.87 mm.

2.5.4 Publications

Davis, K.B., M.-O. Mewes, M.R. Andrews, N.J. van Druten, D.S. Durfee, D.M. Kurn, and W. Ketterle. "Bose-Einstein Condensation in a Gas of Sodium Atoms." *Phys. Rev. Lett.* 75: 3969-3973 (1995).

Davis, K.B., M.-O. Mewes, M.A. Joffe, M.R. Andrews, and W. Ketterle. "Evaporative Cooling of Sodium Atoms." *Phys. Rev. Lett.* 74: 5202 (1995); Erratum: *Phys. Rev. Lett.* 75: 2909 (1995).

Davis, K.B., M.-O. Mewes, and W. Ketterle: "An Analytical Model for Evaporative Cooling of Atoms." *Appl. Phys.* B 60: 155-159 (1995).

Conference Contributions with Published Abstracts

Davis, K.B., M.-O. Mewes, M.A. Joffe, M.R. Andrews, and W. Ketterle. "Evaporative Cooling of Sodium Atoms." In *Research Conference on Bose-Einstein Condensation,* Mont Ste. Odile, June 1995, *Book of Abstracts,* p. 53.

Ketterle, W. "Evaporative Cooling of Magnetically Trapped Sodium." *Bull. Am. Phys. Soc.* 40: 1269 (1995).

Theses

Davis, K.B. *Evaporative Cooling of Sodium Atoms.* Ph.D. diss., Dept. of Physics, MIT, 1995.

Entin, I.A. *Magnetic Trapping of Neutral Sodium Atoms.* S.B. thesis, Dept. of Physics, MIT, 1995.

Thompson, S.H., Jr. *Radio Frequency Induced Evaporative Cooling of Magnetically Trapped Neutral Sodium Atoms.* S.B. thesis, Dept. of Physics, MIT, 1995.

Yesley, P.S. *The Design and Testing of Novel, Spin-Flip, Zeeman Slowing Technique.* S.B. thesis, Dept. of Physics, MIT, 1995.